DOI: 10.13009/EUCASS2019-35

Research on Mechanical Environment Prediction Method for Structure Considering Random Uncertain Elastic Joint

Jiangpan Chen, Dong Wang**, Yan Liu***, Weiwen Zhang****, Yi Liu*****, Limin Sun*******
Beijing Institute of Electronic System Engineering
No. 50 of Yongding Road, Haidian District, Beijing 100854, China
**chenjiangpan@126.com, **13520505058@163.com, ***erica8027@163.com, ****504935834@126.com, *****1037256079@qq.com, ******hebeisunlimin@163.com*

Abstract

In this project, via using none-mass spatial beam element with random uncertain material parameters to simulate the random uncertain elastic joint in complex structure, a high-efficient method, named FICMS-RFM, for calculating the natural frequency of complex structure with random uncertain elastic joint is proposed according to both Fixed Interface Component Mode Synthesis Method (FICMSM) and Random Factor Method (RFM). Firstly, via dividing the elastic joint as an independent substructure and using spatial beam element to simulate it, the natural frequency of a structure considering elastic joint is deduced based on FICMSM. Secondly, to equal the random uncertainty of elastic joint with the random uncertain material parameters of spatial beam element, the natural frequency of a structure considering elastic joint with random uncertainty is achieved according to RFM. Lastly, an example structure with random uncertain elastic joint is designed to verify the proposed FICMS-RFM. The calculation results of the first 10 order natural frequencies of the example structure achieved via FICMS-RFM are compared with them obtained by Monte-Carlo simulation method. The comparison results show that, the relative calculation error of expectation and standard deviation, obtained via FICMS-RFM, is within ±0.033% and ±0.938% respectively.

1. Introduction

There are a number of joints existing in modern engineering complex structures, such as aircraft and spacecraft. However, in actual engineering, all the joints are just elastic connection with high stiffness, not ideally rigid connection [1-2]. The existence of the elasticity of joint has a significant effect on the dynamic properties of the complex structure. In addition, many parameters of the elastic joint in actual engineering, for example material parameters and geometric dimensions, hold random uncertainty. As a consequence, for precisely researching the stiffness of elastic joint, the random uncertainty should be taken into consideration [3-4]. Since the precise prediction of the mechanical environment of complex structure with random uncertain elastic joint is the key to carry out both structural optimization and anti-vibration design for improving both the vibration environmental adaptability and reliability of complex structure, to study the corresponding prediction method has certain engineering meaning.

Component Mode Synthesis (CMS) is a high-efficiency analytical method for obtaining the dynamical properties of large complex structure [5]. By using the low-order reservation main mode and constraint mode (or adherence mode) of each substructure to constitute the Ritz basis of the coupled complex structure, CMS is able to substantially reduce the calculation scale of the finite element model of the structure, with assuring the calculating accuracy, to improve the calculation efficiency [6-7]. The frequently used CMS can be divided into three different methods, namely Fixed Interface Component Mode Synthesis Method (FICMSM), Free Interface Component Mode Synthesis Method and Hybrid Interface Component Mode Synthesis Method [8]. Among them, FICMSM was initially proposed by Hurty in 1965, and then improved by Craig and Bampton [9]. Since high calculation efficiency and easy implementation, FICMSM is widely utilized in actual engineering [8]. In reference [10], by using 6-DOF (degree of freedom) scalar spring system to simulate the elastic joint in complex structure, the dynamic properties of a structure considering elastic joint was investigated on the basis of FICMSM. Since there may be coupling effect between each DOF of elastic joint stiffness in actual engineering, 6-DOF scalar spring system is not in a position to simulate elastic joint precisely. In reference [11] argued that, since the existence of coupling effect between vertical translation DOF and bending DOF, the stiffness of spatial beam element can simulate elastic joint more precisely.

DOI: 10.13009/EUCASS2019-35

RFM is a probabilistic method for high-efficiency handling uncertain problems [12]. The working principle of RFM is to decompose the random uncertain parameter into the product of a random factor and a deterministic parameter, in which the random uncertainty of the random parameter is represented via the random factor. Meanwhile, the mean value of the random factor is 1 and its coefficient of variation is equal to it of the random uncertain parameter [3]. Thus far, lots of achievements, about using RFM to analyze the vibration problems of a structure with random uncertain parameters, have been obtained. In reference [13], the vibration frequency properties of plane steel frame structure with random parameters were studied based on RFM. In reference [14], the natural frequency, modal shape and random vibration response of random truss structure were calculated through RFM. In reference [15], the dynamic properties of piezoelectric intelligent truss structure with random parameters were investigated on the basis of RFM. Via using RFM, in reference [16], the dynamic response properties of random frame structure under the action of an unsteady random excitation were studied. Last but not least, in reference [17], both the natural frequency and modal shape of truss structure with random uncertain material parameters and geometric dimensions were obtained according to RFM. Additionally, RFM was verified via comparing the calculation results obtained from RFM with them form Monte-Carlo simulation method.

In this project, via using none-mass spatial beam element with random uncertain material parameters to simulate the random uncertain elastic joint in complex structure, on the basis of both FICMSM and RFM we propose a high-efficiency method, named FICMS-RFM, to calculate the natural frequency of complex structure considering random uncertain elastic joint. Meanwhile, the proposed FICMS-RFM is verified through numerical simulation. All the conclusions derived from this work have certain theoretical research and engineering application value.

2. Natural Frequency of Structure Considering Uncertain Elastic Joint

Assume the coupling structure to be researched is composed of two subsystems, *A* and *B* as demonstrated in Fig. 1, in which the two substructures are connected via *n* same elastic joints (namely a_i~b_i, i=1,2,…,n) with uncertainty.

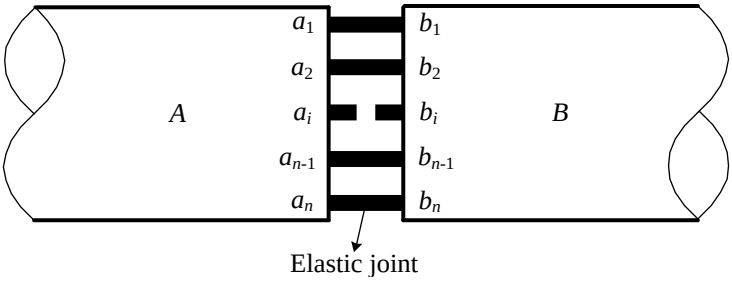

Figure 1: Schematic diagram of the coupling structure to be researched

In general, on the basis of CMS, the coupling structure shown in Fig. 1 can be divided into two substructures (namely Substructure-*A* and Substructure-*B*). The interface node sets of the two substructures are as follows:

$$A_v = \{a_i \,|\, i = 1,2,\cdots,n\}; B_v = \{b_i \,|\, i = 1,2,\cdots,n\} \quad \textbf{(1)}$$

where A_v and B_v represent the interface node set of Substructure-*A* and Substructure-*B*, respectively.

However, for CMS the interface displacement coordination condition of adjacent substructures is required [18]. As for the coupling structure illustrated in Fig. 1, the displacement of the corresponding node a_i and b_i, in A_v and B_v respectively, is not continuous because of the elasticity of the joint. Thus, to analyze the dynamic properties of the coupling structure shown in Fig.1 via using CMS directly may achieve a high-error or even incorrect result. In reference [19] argued that, to consider the elastic joint as an independent connection substructure with only interface nodes would not only follow the substructure division principle of CMS, but also overcome the displacement inconsistency of the interface node of Substructure-*A* and Substructure-*B*. In this project, therefore, the coupling structure shown in Fig. 1 is divided into three substructures (two primary substructures Substructure-*A* and Substructure-*B*, and a connecting substructure Substructure-*C*) for using FICMSM to analyze its dynamic properties as demonstrated in Fig. 2.

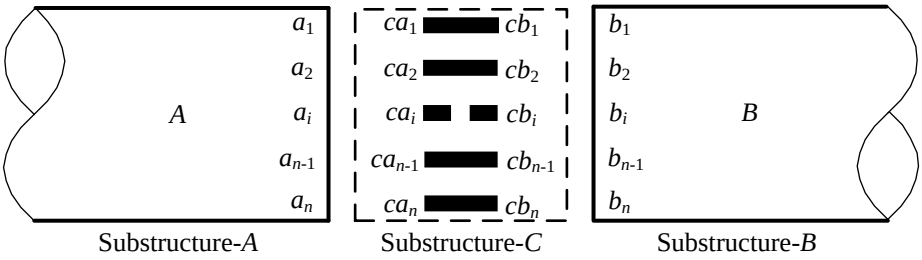

Figure 2: Schematic diagram of the divided substructures

DOI: 10.13009/EUCASS2019-35

According to the working principle of FICMSM [18], firstly, both the mass matrix and stiffness matrix of Substructure-*t* (*t*=*A*, *B*) should be arranged as follows:

$$\boldsymbol{M}^{t}=\begin{bmatrix}\boldsymbol{M}_{uu}^{t} & \boldsymbol{M}_{uv}^{t}\\ \boldsymbol{M}_{vu}^{t} & \boldsymbol{M}_{vv}^{t}\end{bmatrix};\boldsymbol{K}^{t}=\begin{bmatrix}\boldsymbol{K}_{uu}^{t} & \boldsymbol{K}_{uv}^{t}\\ \boldsymbol{K}_{vu}^{t} & \boldsymbol{K}_{vv}^{t}\end{bmatrix} \tag{2}$$

where $\boldsymbol{M}^{t}$ and $\boldsymbol{K}^{t}$ represent the mass matrix and stiffness matrix of Substructure-*t* respectively, *u* and *v* denote the internal node DOF and interface node DOF respectively.

For two primary substructures, the normal mode set and constrained mode set of Substructure-*t* are given by [18]:

$$\begin{aligned}&\boldsymbol{\varphi}_{n}^{t}=\begin{bmatrix}\boldsymbol{\varphi}_{un}^{t}\\ \boldsymbol{0}_{vn}\end{bmatrix};\left(\boldsymbol{K}_{uu}^{t}-\omega^{2}\boldsymbol{M}_{uu}^{t}\right)\boldsymbol{\varphi}_{un}^{t}=\boldsymbol{0}\\ &\boldsymbol{\varphi}_{c}^{t}=\begin{bmatrix}\boldsymbol{\varphi}_{uc}^{t}\\ \boldsymbol{I}_{vc}\end{bmatrix};\boldsymbol{\varphi}_{uc}^{t}=-\left(\boldsymbol{K}_{uu}^{t}\right)^{-1}\boldsymbol{K}_{uv}^{t}\end{aligned} \tag{3}$$

where $\boldsymbol{\varphi}_{n}^{t}$ and $\boldsymbol{\varphi}_{c}^{t}$ index the normal mode set and constrained mode set of Substructure-*t* respectively, ω and $\boldsymbol{I}$ yield the angular frequency and unit matrix respectively. According to Eq. (3), therefore, we can obtain the assumed mode set of the primary Substructure-*t* as:

$$\boldsymbol{\varphi}^{t}=\begin{bmatrix}\boldsymbol{\varphi}_{nk}^{t} & \boldsymbol{\varphi}_{c}^{t}\end{bmatrix}=\begin{bmatrix}\boldsymbol{\varphi}_{unk}^{t} & \boldsymbol{\varphi}_{uc}^{t}\\ \boldsymbol{0}_{vnk} & \boldsymbol{I}_{vc}\end{bmatrix} \tag{4}$$

where $\boldsymbol{\varphi}^{t}$ is the assumed mode set of Substructure-*t* that used to participate the mode synthesis, *k* is the reserved normal mode order of Substructure-*t*. Generally, *k* is less far than *w* (the overall normal mode order of substructure-*t*), and this explains why FICMSM is more efficient than traditional Finite Element Method (FEM).

For connecting substructure Substructure-*C*, since there is only interface node, we use spatial beam element to simulate the stiffness of elastic joint. In addition, the material parameters (both Young's modulus *E* and Poisson's ratio γ) with random uncertainty are used to simulate the random uncertainty of the elastic joint. Then according to reference [20], the stiffness matrix of the spatial beam element can be redefined as:

$$\boldsymbol{K}_{b}=E\boldsymbol{K}_{b1}+\frac{E}{1+\gamma}\boldsymbol{K}_{b2} \tag{5}$$

where $\boldsymbol{K}_{b}$ indexes the stiffness matrix of spatial beam element, both $\boldsymbol{K}_{b1}$ and $\boldsymbol{K}_{b2}$ are matrices without uncertainty and the corresponding expressions are as follows:

$$\boldsymbol{K}_{b1}=\begin{bmatrix}\boldsymbol{K}_{11} & \boldsymbol{K}_{12}^{\mathrm{T}}\\ \boldsymbol{K}_{12} & \boldsymbol{K}_{13}\end{bmatrix};\boldsymbol{K}_{b2}=\begin{bmatrix}\boldsymbol{K}_{21} & -\boldsymbol{K}_{21}\\ -\boldsymbol{K}_{21} & \boldsymbol{K}_{21}\end{bmatrix}$$

$$\boldsymbol{K}_{11}=\frac{1}{L^{3}}\begin{bmatrix}SL^{2} & 0 & 0 & 0 & 0 & 0\\ 0 & 12I_{z} & 0 & 0 & 0 & 6I_{z}L\\ 0 & 0 & 12I_{y} & 0 & -6I_{y}L & 0\\ 0 & 0 & 0 & 0 & 0 & 0\\ 0 & 0 & -6I_{y}L & 0 & 4I_{y}L^{2} & 0\\ 0 & 6I_{z}L & 0 & 0 & 0 & 4I_{z}L^{2}\end{bmatrix};\boldsymbol{K}_{12}=\frac{1}{L^{3}}\begin{bmatrix}-SL^{2} & 0 & 0 & 0 & 0 & 0\\ 0 & -12I_{z} & 0 & 0 & 0 & -6I_{z}L\\ 0 & 0 & -12I_{y} & 0 & 6I_{y}L & 0\\ 0 & 0 & 0 & 0 & 0 & 0\\ 0 & 0 & -6I_{y}L & 0 & 2I_{y}L^{2} & 0\\ 0 & 6I_{z}L & 0 & 0 & 0 & 2I_{z}L^{2}\end{bmatrix}$$

$$\boldsymbol{K}_{13}=\frac{1}{L^{3}}\begin{bmatrix}SL^{2} & 0 & 0 & 0 & 0 & 0\\ 0 & 12I_{z} & 0 & 0 & 0 & -6I_{z}L\\ 0 & 0 & 12I_{y} & 0 & 6I_{y}L & 0\\ 0 & 0 & 0 & 0 & 0 & 0\\ 0 & 0 & 6I_{y}L & 0 & 4I_{y}L^{2} & 0\\ 0 & -6I_{z}L & 0 & 0 & 0 & 4I_{z}L^{2}\end{bmatrix};\boldsymbol{K}_{21}=\frac{1}{2L}\begin{bmatrix}0 & 0 & 0 & 0 & 0 & 0\\ 0 & 0 & 0 & 0 & 0 & 0\\ 0 & 0 & 0 & 0 & 0 & 0\\ 0 & 0 & 0 & I_{x} & 0 & 0\\ 0 & 0 & 0 & 0 & 0 & 0\\ 0 & 0 & 0 & 0 & 0 & 0\end{bmatrix} \tag{6}$$

where *S* and *L* denote sectional area and element length of spatial beam element, respectively, I_x indicates the second polar moment of area of the spatial beam element, I_y and I_z index the second Y-axial and Z-axial moment of area of spatial beam element, respectively. As a consequence, the stiffness matrix of the connecting substructure Substructure-*C* can be obtained as:

$$\begin{aligned}&\boldsymbol{K}^{C}=\boldsymbol{G}\left[\operatorname{diag}\left(\boldsymbol{K}_{b},\cdots,\boldsymbol{K}_{b}\right)\right]\boldsymbol{G}^{\mathrm{T}}=E\boldsymbol{K}_{1}^{C}+\frac{E}{1+\gamma}\boldsymbol{K}_{2}^{C}\\ &\boldsymbol{K}_{1}^{C}=\boldsymbol{G}\left[\operatorname{diag}\left(\boldsymbol{K}_{b1},\cdots,\boldsymbol{K}_{b1}\right)\right]\boldsymbol{G}^{\mathrm{T}};\boldsymbol{K}_{2}^{C}=\boldsymbol{G}\left[\operatorname{diag}\left(\boldsymbol{K}_{b2},\cdots,\boldsymbol{K}_{b2}\right)\right]\boldsymbol{G}^{\mathrm{T}}\end{aligned} \tag{7}$$

where $\boldsymbol{G}$ is a transformation matrix whose expression can be found in reference [21]. Meanwhile, $\boldsymbol{G}$, $\boldsymbol{K}_{1}^{C}$ and $\boldsymbol{K}_{2}^{C}$ are

DOI: 10.13009/EUCASS2019-35

all matrices without uncertainty.

Regarding to the mass of Substructure-*C*, since it is so trivial, comparing with the overall coupling structure, that can be ignored [10, 21]. Then we can define the corresponding mass matrix $\boldsymbol{M}^{C}$ as:

$$\boldsymbol{M}^{C} = \boldsymbol{0} \tag{8}$$

Additionally, as spatial beam element possesses only interface nodes, there is only constrained mode set in the assumed mode set of Substructure-*C* on the basis of Eq. (3). The assumed mode set of Substructure-*C* is given by:

$$\boldsymbol{\varphi}^{C} = \boldsymbol{\varphi}_{c}^{C} = \boldsymbol{I} \tag{9}$$

where $\boldsymbol{\varphi}^{C}$ and $\boldsymbol{\varphi}_{c}^{C}$ are the assumed mode set and constrained mode set of Substructure-*C*, respectively.

Based on what have been discussed above, the mass matrix $\boldsymbol{M}$, stiffness matrix $\boldsymbol{K}$ and mode set $\boldsymbol{\varphi}$ of the coupling structure are as follows:

$$\boldsymbol{M} = \begin{bmatrix} \boldsymbol{M}^{A} & \boldsymbol{0} & \boldsymbol{0} \\ \boldsymbol{0} & \boldsymbol{M}^{C} & \boldsymbol{0} \\ \boldsymbol{0} & \boldsymbol{0} & \boldsymbol{M}^{B} \end{bmatrix} = \begin{bmatrix} \boldsymbol{M}^{A} & \boldsymbol{0} & \boldsymbol{0} \\ \boldsymbol{0} & \boldsymbol{0} & \boldsymbol{0} \\ \boldsymbol{0} & \boldsymbol{0} & \boldsymbol{M}^{B} \end{bmatrix}; \boldsymbol{K} = \begin{bmatrix} \boldsymbol{K}^{A} & \boldsymbol{0} & \boldsymbol{0} \\ \boldsymbol{0} & \boldsymbol{K}^{C} & \boldsymbol{0} \\ \boldsymbol{0} & \boldsymbol{0} & \boldsymbol{K}^{B} \end{bmatrix}; \boldsymbol{\varphi} = \begin{bmatrix} \boldsymbol{\varphi}^{A} & \boldsymbol{0} & \boldsymbol{0} \\ \boldsymbol{0} & \boldsymbol{\varphi}^{C} & \boldsymbol{0} \\ \boldsymbol{0} & \boldsymbol{0} & \boldsymbol{\varphi}^{B} \end{bmatrix} \tag{10}$$

Assume that the displacement vector corresponding to Eq. (10) is $\boldsymbol{U}$, which is given by:

$$\boldsymbol{U} = \begin{bmatrix} \boldsymbol{U}_{Au}^{\mathrm{T}} & \boldsymbol{U}_{Av}^{\mathrm{T}} & \boldsymbol{U}_{CAv}^{\mathrm{T}} & \boldsymbol{U}_{CBv}^{\mathrm{T}} & \boldsymbol{U}_{Bu}^{\mathrm{T}} & \boldsymbol{U}_{Bv}^{\mathrm{T}} \end{bmatrix}^{\mathrm{T}} \tag{11}$$

where $\boldsymbol{U}_{tu}$ and $\boldsymbol{U}_{tv}$ yield the internal node and interface node displacement of Substructure-*t* respectively, $\boldsymbol{U}_{Ctv}$ is the interface node displacement of Substructure-*C* corresponding to the primary substructure Substructure-*t*. Then according to Eq. (10), modal coordinate transformation is performed on $\boldsymbol{U}$, which is indexed as:

$$\boldsymbol{U} = \boldsymbol{\varphi}\boldsymbol{P} \tag{12}$$

where $\boldsymbol{P}$ is the modal coordinate corresponding to mode set $\boldsymbol{\varphi}$, and the expression is as:

$$\boldsymbol{P} = \begin{bmatrix} \boldsymbol{P}_{An}^{\mathrm{T}} & \boldsymbol{P}_{Ac}^{\mathrm{T}} & \boldsymbol{P}_{CAc}^{\mathrm{T}} & \boldsymbol{P}_{CBc}^{\mathrm{T}} & \boldsymbol{P}_{Bn}^{\mathrm{T}} & \boldsymbol{P}_{Bc}^{\mathrm{T}} \end{bmatrix}^{\mathrm{T}} \tag{13}$$

where $\boldsymbol{P}_{tn}$ and $\boldsymbol{P}_{tc}$ are the modal coordinates corresponding to the reserved normal mode set and constrained mode set of Substructure-*t* respectively, $\boldsymbol{P}_{Ctc}$ is the modal coordinate corresponding to the constrained mode set of Substructure-*C*. Meanwhile, the modal mass matrix $\boldsymbol{M}_{\boldsymbol{P}}$ and modal stiffness matrix $\boldsymbol{K}_{\boldsymbol{P}}$ of the coupling structure corresponding to the modal coordinate $\boldsymbol{P}$ are as follows:

$$\boldsymbol{M}_{\boldsymbol{P}} = \boldsymbol{\varphi}^{\mathrm{T}}\boldsymbol{M}\boldsymbol{\varphi}; \boldsymbol{K}_{\boldsymbol{P}} = \boldsymbol{\varphi}^{\mathrm{T}}\boldsymbol{K}\boldsymbol{\varphi} \tag{14}$$

The interface displacement coordination condition is given by:

$$\boldsymbol{U}_{CAv} = \boldsymbol{L}_{A}\boldsymbol{U}_{Av}; \boldsymbol{U}_{CBv} = \boldsymbol{L}_{B}\boldsymbol{U}_{Bv} \tag{15}$$

where $\boldsymbol{L}_{\boldsymbol{A}}$ and $\boldsymbol{L}_{\boldsymbol{B}}$ are both coordinate rotation transformation matrices. From Eqs. (4), (9) to (13) and (15) we can obtain that:

$$\boldsymbol{P}_{CAc} = \boldsymbol{L}_{A}\boldsymbol{P}_{Ac}; \boldsymbol{P}_{CBc} = \boldsymbol{L}_{B}\boldsymbol{P}_{Bc} \tag{16}$$

Via observing Eq. (16) we can learn that the element of modal coordinate $\boldsymbol{P}$ is not independent of each other. Therefore, independent transformation must be acted on the modal coordinate $\boldsymbol{P}$ through introducing the transformation matrix $\boldsymbol{E}$. The transformation process is as follows:

$$\boldsymbol{P} = \boldsymbol{E}\boldsymbol{Q} = \begin{bmatrix} \boldsymbol{I} & \boldsymbol{0} & \boldsymbol{0} & \boldsymbol{0} \\ \boldsymbol{0} & \boldsymbol{I} & \boldsymbol{0} & \boldsymbol{0} \\ \boldsymbol{0} & \boldsymbol{L}_{P} & \boldsymbol{0} & \boldsymbol{0} \\ \boldsymbol{0} & \boldsymbol{0} & \boldsymbol{0} & \boldsymbol{L}_{Q} \\ \boldsymbol{0} & \boldsymbol{0} & \boldsymbol{I} & \boldsymbol{0} \\ \boldsymbol{0} & \boldsymbol{0} & \boldsymbol{0} & \boldsymbol{I} \end{bmatrix} \begin{bmatrix} \boldsymbol{P}_{An} \\ \boldsymbol{P}_{Ac} \\ \boldsymbol{P}_{Bn} \\ \boldsymbol{P}_{Bc} \end{bmatrix}; \boldsymbol{E} = \begin{bmatrix} \boldsymbol{I} & \boldsymbol{0} & \boldsymbol{0} & \boldsymbol{0} \\ \boldsymbol{0} & \boldsymbol{I} & \boldsymbol{0} & \boldsymbol{0} \\ \boldsymbol{0} & \boldsymbol{L}_{P} & \boldsymbol{0} & \boldsymbol{0} \\ \boldsymbol{0} & \boldsymbol{0} & \boldsymbol{0} & \boldsymbol{L}_{Q} \\ \boldsymbol{0} & \boldsymbol{0} & \boldsymbol{I} & \boldsymbol{0} \\ \boldsymbol{0} & \boldsymbol{0} & \boldsymbol{0} & \boldsymbol{I} \end{bmatrix}; \boldsymbol{Q} = \begin{bmatrix} \boldsymbol{P}_{An} \\ \boldsymbol{P}_{Ac} \\ \boldsymbol{P}_{Bn} \\ \boldsymbol{P}_{Bc} \end{bmatrix} \tag{17}$$

In Eq. (17), $\boldsymbol{Q}$ is the independent modal coordinate of the coupling structure. In addition, the modal mass matrix $\boldsymbol{M}_{\boldsymbol{Q}}$ and modal stiffness matrix $\boldsymbol{K}_{\boldsymbol{Q}}$ of the coupling structure corresponding to the modal coordinate $\boldsymbol{Q}$ are as follows:

$$\boldsymbol{M}_{Q} = \boldsymbol{S}^{\mathrm{T}}\boldsymbol{\varphi}^{\mathrm{T}}\boldsymbol{M}\boldsymbol{\varphi}\boldsymbol{S}; \boldsymbol{K}_{Q} = \boldsymbol{S}^{\mathrm{T}}\boldsymbol{\varphi}^{\mathrm{T}}\boldsymbol{K}\boldsymbol{\varphi}\boldsymbol{S} \tag{18}$$

From what have been discussed above, therefore, we can define the undamped free vibration equation of the coupling structure as:

$$\boldsymbol{M}_{Q}\ddot{\boldsymbol{Q}} + \boldsymbol{K}_{Q}\boldsymbol{Q} = \boldsymbol{0} \tag{19}$$

Assume that the mode set of Eq. (19) is $\boldsymbol{\psi}$, which can be calculated via:

$$\left(\boldsymbol{K}_{Q} - \omega^{2}\boldsymbol{M}_{Q}\right)\boldsymbol{\psi} = \boldsymbol{0}; \boldsymbol{\psi} = \begin{bmatrix} \boldsymbol{\psi}_{1} & \cdots & \boldsymbol{\psi}_{i} & \cdots \end{bmatrix} \tag{20}$$

where $\boldsymbol{\psi}_{\boldsymbol{i}}$ is the *i*-th order modal shape corresponding to Eq. (19). Therefore, according to Rayleigh quotient formula, we can obtain the natural frequency of the coupling structure considering uncertain elastic joint demonstrated in Fig. 1 as:

DOI: 10.13009/EUCASS2019-35

$$\omega_i^2 = \frac{\boldsymbol{\psi}_i^{\mathrm{T}} \boldsymbol{K}_Q \boldsymbol{\psi}_i}{\boldsymbol{\psi}_i^{\mathrm{T}} \boldsymbol{M}_Q \boldsymbol{\psi}_i} = \frac{\boldsymbol{\psi}_i^{\mathrm{T}} \boldsymbol{S}^{\mathrm{T}} \boldsymbol{\varphi}^{\mathrm{T}} \boldsymbol{K}_{ab} \boldsymbol{\varphi} \boldsymbol{S} \boldsymbol{\psi}_i}{\boldsymbol{\psi}_i^{\mathrm{T}} \boldsymbol{S}^{\mathrm{T}} \boldsymbol{\varphi}^{\mathrm{T}} \boldsymbol{M} \boldsymbol{\varphi} \boldsymbol{S} \boldsymbol{\psi}_i} + E \frac{\boldsymbol{\psi}_i^{\mathrm{T}} \boldsymbol{S}^{\mathrm{T}} \boldsymbol{\varphi}^{\mathrm{T}} \boldsymbol{K}_{c1} \boldsymbol{\varphi} \boldsymbol{S} \boldsymbol{\psi}_i}{\boldsymbol{\psi}_i^{\mathrm{T}} \boldsymbol{S}^{\mathrm{T}} \boldsymbol{\varphi}^{\mathrm{T}} \boldsymbol{M} \boldsymbol{\varphi} \boldsymbol{S} \boldsymbol{\psi}_i} + \frac{E}{1+\gamma} \frac{\boldsymbol{\psi}_i^{\mathrm{T}} \boldsymbol{S}^{\mathrm{T}} \boldsymbol{\varphi}^{\mathrm{T}} \boldsymbol{K}_{c2} \boldsymbol{\varphi} \boldsymbol{S} \boldsymbol{\psi}_i}{\boldsymbol{\psi}_i^{\mathrm{T}} \boldsymbol{S}^{\mathrm{T}} \boldsymbol{\varphi}^{\mathrm{T}} \boldsymbol{M} \boldsymbol{\varphi} \boldsymbol{S} \boldsymbol{\psi}_i} \tag{21}$$

where $\boldsymbol{K_{ab}}$, $\boldsymbol{K_{c1}}$ and $\boldsymbol{K_{c2}}$ are all deterministic matrices, and the corresponding expressions are as follows:

$$\boldsymbol{K}_{ab} = \begin{bmatrix} \boldsymbol{K}^{\boldsymbol{A}} & \boldsymbol{0} & \boldsymbol{0} \\ \boldsymbol{0} & \boldsymbol{0} & \boldsymbol{0} \\ \boldsymbol{0} & \boldsymbol{0} & \boldsymbol{K}^{\boldsymbol{B}} \end{bmatrix}; \boldsymbol{K}_{c1} = \begin{bmatrix} \boldsymbol{0} & \boldsymbol{0} & \boldsymbol{0} \\ \boldsymbol{0} & \boldsymbol{K}_1^{\boldsymbol{C}} & \boldsymbol{0} \\ \boldsymbol{0} & \boldsymbol{0} & \boldsymbol{0} \end{bmatrix}; \boldsymbol{K}_{c2} = \begin{bmatrix} \boldsymbol{0} & \boldsymbol{0} & \boldsymbol{0} \\ \boldsymbol{0} & \boldsymbol{K}_2^{\boldsymbol{C}} & \boldsymbol{0} \\ \boldsymbol{0} & \boldsymbol{0} & \boldsymbol{0} \end{bmatrix} \tag{22}$$

3. Fixed Interface Component Mode Synthesis-Random Factor Method

As mentioned above, we set both Young's modulus E and Poisson's ratio γ of Substructure-C to random parameters to simulate the random uncertainty of the elastic joint. In addition, another random parameter β is introduced, of which the expression is β=1+γ. Then based on RFM, the three random parameters can be redefined as [13]:

$$E = E_m E_r; \gamma = \gamma_m \gamma_r; \beta = \beta_m \beta_r = (1+\gamma_m)\beta_r \tag{23}$$

where the subscript m and r yield the mean value and the random factor of the random parameter, respectively. Meanwhile, in reference [13] the expectation μ and standard deviation σ of the random factor were given by:

$$\mu(E_r) = \mu(\beta_r) = \mu(\gamma_r) = 1; \sigma(E_r) = \upsilon_E; \sigma(\gamma_r) = \upsilon_\gamma; \sigma(\beta_r) = \upsilon_\beta \tag{24}$$

where υ denotes the coefficient of variation of the random parameter. The coefficients of variation of the three random parameters can be calculated via:

$$\upsilon_E = \frac{\sigma(E)}{\mu(E)}; \upsilon_\gamma = \frac{\sigma(\gamma)}{\mu(\gamma)}; \upsilon_\beta = \frac{\sigma(\beta)}{\mu(\beta)} \tag{25}$$

Substituting β=1+γ into Eq. (25) we can achieve that:

$$\upsilon_\beta = \frac{\sigma(1+\gamma)}{\mu(1+\gamma)} = \frac{\upsilon_\gamma \gamma_m}{1+\gamma_m} \tag{26}$$

Meanwhile, in the right part of Eq. (21), besides of random parameters E and γ, $\boldsymbol{\psi_i}$ holds random uncertainty as well and can be redefined as:

$$\boldsymbol{\psi}_i = \boldsymbol{\psi}_{im} \psi_{ir} \tag{27}$$

where $\boldsymbol{\psi_{im}}$ and ψ_{ir} yield the mean value and random factor of $\boldsymbol{\psi_i}$. Of them, $\boldsymbol{\psi_{im}}$ can be obtained via substituting both E_m and γ_m into Eq. (20). Consequently, by substituting Eqs. (23) and (27) into Eq. (21) we can get that:

$$\omega_i^2 = \omega_{iab}^2 + E_r \omega_{ic1}^2 + \frac{E_r}{\beta_r} \omega_{ic2}^2 \tag{28}$$

In Eq. (28), ${\omega_{iab}}^2$, ${\omega_{ic1}}^2$ and ${\omega_{ic2}}^2$ are all deterministic parameters, whose expressions are as follows:

$$\omega_{iab}^2 = \frac{\boldsymbol{\psi}_{im}^{\mathrm{T}} \boldsymbol{S}^{\mathrm{T}} \boldsymbol{\varphi}^{\mathrm{T}} \boldsymbol{K}_{ab} \boldsymbol{\varphi} \boldsymbol{S} \boldsymbol{\psi}_{im}}{\boldsymbol{\psi}_{im}^{\mathrm{T}} \boldsymbol{S}^{\mathrm{T}} \boldsymbol{\varphi}^{\mathrm{T}} \boldsymbol{M} \boldsymbol{\varphi} \boldsymbol{S} \boldsymbol{\psi}_{im}}; \omega_{ic1}^2 = E_m \frac{\boldsymbol{\psi}_{im}^{\mathrm{T}} \boldsymbol{S}^{\mathrm{T}} \boldsymbol{\varphi}^{\mathrm{T}} \boldsymbol{K}_{c1} \boldsymbol{\varphi} \boldsymbol{S} \boldsymbol{\psi}_{im}}{\boldsymbol{\psi}_{im}^{\mathrm{T}} \boldsymbol{S}^{\mathrm{T}} \boldsymbol{\varphi}^{\mathrm{T}} \boldsymbol{M} \boldsymbol{\varphi} \boldsymbol{S} \boldsymbol{\psi}_{im}}; \omega_{ic2}^2 = \frac{E_m}{\beta_m} \frac{\boldsymbol{\psi}_{im}^{\mathrm{T}} \boldsymbol{S}^{\mathrm{T}} \boldsymbol{\varphi}^{\mathrm{T}} \boldsymbol{K}_{c2} \boldsymbol{\varphi} \boldsymbol{S} \boldsymbol{\psi}_{im}}{\boldsymbol{\psi}_{im}^{\mathrm{T}} \boldsymbol{S}^{\mathrm{T}} \boldsymbol{\varphi}^{\mathrm{T}} \boldsymbol{M} \boldsymbol{\varphi} \boldsymbol{S} \boldsymbol{\psi}_{im}} \tag{29}$$

Meanwhile, the expectation and standard deviation of ${\omega_i}^2$ as demonstrated in Eq. (28) can be achieved on the basis of algebraic synthesis method [12]. The results are as follows:

$$\begin{cases} \mu_i = \omega_{iab}^2 + \omega_{ic1}^2 + \left(1 + \upsilon_\beta^2 - c\upsilon_E \upsilon_\beta\right)\omega_{ic2}^2 \\ \sigma_i^2 = \left(1 + \upsilon_E^2 + c^2 \upsilon_E^2\right)\upsilon_\beta^2 \omega_{ic2}^4 + \upsilon_E^2 \left[\omega_{ic1}^2 + \left(1+\upsilon_\beta^2\right)\omega_{ic2}^2\right]^2 - 2c\upsilon_E \upsilon_\beta \left[\omega_{ic1}^2 + \left(1+\upsilon_\beta^2\right)\omega_{ic2}^2\right]\omega_{ic2}^2 \end{cases} \tag{30}$$

where c is the correlation coefficient between random parameters E and γ.

As a result, on the basis of Eq. (30), we can achieve the expectation and standard deviation of the i-th order natural frequency f_i of the coupling structure considering random uncertain elastic joint demonstrated in Fig. 1 as:

$$\mu(f_i) = \frac{1}{2\pi} \sqrt[4]{\mu_i^2 - \frac{\sigma_i^2}{2}}; \sigma(f_i) = \frac{1}{2\pi} \sqrt{\mu_i - \sqrt{\mu_i^2 - \frac{\sigma_i^2}{2}}} \tag{31}$$

What have been discussed above can be defined as the derivation process of FICMS-RFM.

4. Numerical Simulation

An example structure with random uncertain elastic joint, as illustrated in Fig. 3, is designed to verify the proposed FICMS-RFM via using both FICMS-RFM and Monte-Carlo simulation method to calculate the natural frequency of the designed structure.

DOI: 10.13009/EUCASS2019-35

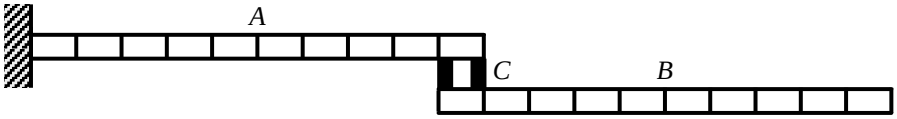

Figure 3: Schematic diagram of the example structure

In Fig. 3, *A* and *B* are the exactly same two rectangular cross-section beams (0.02×0.04 m^2 in cross-section area and 0.5 m in length); *C* is the elastic joint with random uncertainty which is simulated by two same circular cross-section short beams (0.005 m in cross-section diameter and 0.05 m in length) with random uncertain Young's modulus *E* and Poisson's ratio γ. Spatial beam element is used to mesh *A*, *B*, *C* and the whole example structure. The element properties of the deterministic structures *A* and *B* and the random uncertain structure *C* are listed in Tab. 1 and Tab. 2, respectively.

Table 1: Element properties of the deterministic structures *A* and *B*

	E	γ	ρ	L	Element Number
Value [Unit]	7×10^{10} [Pa]	0.3	2700 [kg/m^3]	0.05 [m]	10

Table 2: Element properties of the random uncertain elastic joint *C*

	E_m	υ_E	γ_m	υ_γ	c	ρ	L	Element Number
Value [Unit]	2.1×10^{11} [Pa]	0.05	0.3	0.1	0	0 [kg/m^3]	0.05 [m]	2

According to the data listed in Tab. 2 we can learn that:

$$\beta_m = 1.3; \upsilon_\beta = 0.023 \tag{32}$$

Via using FICMS-RFM to calculate the natural frequency, the example structure is divided into three substructures (namely Substructure-*A*, Substructure-*B* and Substructure-*C*), and the former 30 order normal modes of both substructure-*A* and substructure-*B* are taken as the reserved normal mode set of corresponding substructure.

For using Monte-Carlo simulation method to calculate the natural frequency, firstly, assume that both the random parameters *E* and γ obey normal distribution; secondly, randomly generating 20000 samples based on the digital characteristics of the normal distribution; thirdly, substituting the 20000 samples into the finite element model of the whole example structure respectively and then calculating the natural frequency 20000 times; lastly, using the 20000 calculation results to calculate the expectation μ and standard deviation σ of the natural frequency. Meanwhile, the expectation μ and standard deviation σ of the two parameters obeying normal distribution are as follows [22]:

$$\begin{cases} \mu(E) = E_M \\ \sigma(E) = \upsilon_E E_M \end{cases}; \begin{cases} \mu(\gamma) = \gamma_M \\ \sigma(\gamma) = \upsilon_\gamma \gamma_M \end{cases} \tag{33}$$

The calculation results of the former 10 order natural frequencies achieved via both FICMS-RFM and Monte-Carlo simulation method are demonstrated in Tab. 3. In Tab. 3, μ^{MC}, σ^{MC} and μ^{FR}, σ^{FR} yield the calculation results of the expectation and standard deviation of the natural frequency obtained via Monte-Carlo simulation method and FICMS-RFM, respectively. Assume the calculation results achieved by Monte-Carlo simulation method are the reference value, ε_μ and ε_σ index the relative calculation error of the expectation and standard deviation obtained via FICMS-RFM respectively.

From Tab. 3 we can learn that, the relative calculation error of expectation and standard deviation, obtained via FICMS-RFM, is within ±0.033% and ±0.938% respectively. As a consequence, via using none-mass spatial beam element with random uncertain material parameters to simulate the random uncertain elastic joint in complex structure, FICMS-RFM holds the ability to predict the mechanical environment of complex structure with random uncertain elastic joint correctly and efficiently.

5. Conclusions

Via using none-mass spatial beam element with random uncertain material parameters to simulate the random uncertain elastic joint in complex structure, the natural frequency of a structure considering uncertain elastic joint is deduced on the basis of FICMSM. Based on the deduction results, a high-efficiency method FICMS-RFM for calculating the natural frequency of a structure considering random uncertain elastic joint is proposed according to RFM. Simulation results indicate that, while greatly improving calculation efficiency, FICMS-RFM can still guarantee high calculation accuracy. As a consequence, via using none-mass spatial beam element with random

DOI: 10.13009/EUCASS2019-35

uncertain material parameters to simulate the random uncertain elastic joint in complex structure, FICMS-RFM holds the ability to predict the mechanical environment of a complex structure with random uncertain elastic joint correctly and efficiently. All the conclusions obtained from this project are meaningful for theoretical investigation and engineering application.

Table 3: Calculation results of the natural frequency

	μ^{MC}[Hz]	μ^{FR}[Hz]	ε_{μ}[%]	σ^{MC}[Hz]	σ^{FR}[Hz]	ε_{σ}[%]
1st order	15.860	15.863	0.019	0.320	0.323	0.938
2nd order	17.934	17.934	0.000	0.004	0.004	0.000
3rd order	89.862	89.882	0.022	0.834	0.838	0.480
4th order	108.355	108.361	0.006	0.122	0.122	0.000
5th order	161.981	162.003	0.014	3.520	3.546	0.739
6th order	183.161	183.171	0.005	2.915	2.939	0.823
7th order	329.341	329.334	-0.002	0.640	0.646	0.938
8th order	544.409	544.591	0.033	8.196	8.236	0.488
9th order	597.231	597.264	0.006	0.740	0.739	-0.135
10th order	840.116	840.119	0.000	0.482	0.486	0.830

References

[1] Chen, L. M. 2005. Spacecraft Structures and Mechanisms. China Science and Technology Press.

[2] Zou, Y. J. 2010. Bush Finite Element Principle and Its Application in Building Structural Models for Spacecraft. *Spacecraft Engineering*. 19: 99-105.

[3] Lin, L. G., and Chen J. J. 2009. A Method of Dynamic Characteristic Analysis of Interval stochastic Truss Structures. *Journal of Vibration and Shock*. 28: 65-69.

[4] Daouk, S., Louf, F., and Dorival, O., et al. 2015. Uncertainties in Structural Dynamics: Overview and Comparative Analysis of Methods. *Mechanics & Industry*. 16: 1-10.

[5] Lou, M. L. 1995. Link Substructure and Modal Synthesis for Substructuring. *Journal of Vibration Engineering*. 8: 52-56.

[6] Wang, X. H., An, F., and Cao, L. J., et al. 2009. Direct Transformation Method for Mode Synthesis. *Acta Aeronautica et Astronautica Sinica*. 30: 92-98.

[7] Hinke, L., Dohnal, F., and Mace, B. R., et al. 2009. Component Mode Synthesis as a Framework for Uncertainty Analysis. J*ournal of Sound and Vibration*. 324: 161-178.

[8] Li, X. Q., Deng, Z. X., and Pang, J., et al. 2012. Ritz Transform Method for Interface Degree of Freedom of Modal Synthesis. *Journal of South China University of Technology (Natural Science Edition)*. 40: 111-116.

[9] Wang, M., and Zheng, G. T. 2012. An Improved Fixed-interface Modal Synthesis Method. *Journal of Astronautics*. 33: 291-297.

[10] Li, X. H., and Yang, B. Y. 1987. The Connecting Substructures in the Analysis of Structural Vibrations. *Journal of Astronautics*. 1: 7-15.

[11] Li, K. 2016. Research on Spacecraft Section Vibration Environment Prediction Methods. Master Thesis. Nanjing University of Aeronautics and Astronautics.

[12] Gao, W. 2007. Natural Frequency and Mode Shape Analysis of Structures with Uncertainty. *Mechanical Systems and Signal Processing*. 21: 24-39.

[13] Hu, T. B., Chen, J. J., and Xu, Y. L. 2006. Random Factor Method for Frequency Characteristic Analysis of Stochastic Frame Structures. *Journal of Mechanical Strength*. 28: 196-200.

[14] Gao, W., Zhang, N., and Ji, J. 2009. A New Method for Random Vibration Analysis of Stochastic Truss Structures. *Finite Elements in Analysis and Design*. 45: 190-199.

DOI: 10.13009/EUCASS2019-35

[15] Gao, W., Chen, J. J., and Liu, W., et al. 2003. Dynamic Characteristics Analysis for Intelligent Truss Structures with Random Parameters. *Chinese Journal of Applied Mechanics*. 20: 123-127.
[16] Gao, W., Chen, J. J., and Ma, J., et al. 2004. Dynamic Response Analysis of Stochastic Frame Structures Under Nonstationary Random Excitation. *AIAA Journal*. 42: 1818-1822.
[17] Fan, Z. B. 2011. Dynamics Analysis Technique Research of Structure with Uncertainty. Master Thesis. Nanjing University of Aeronautics and Astronautics.
[18] Wang, Y. Y. 1999.Theory and Application of Dynamic Substructure method. Science Press.
[19] Zhang, H. T., Zhang, Z. H., and Wang, Z. Q., et al. 1994. Connection Substructure in Free-interface Mode Synthesis Technique. *Journal of Vibration and Shock*. 13: 55-59.
[20] Xing, Y. F., and Li, M. 2011. Principles and Methods of Computational Solid Mechanics. Beijing University of Aeronautics and Astronautics Press.
[21] Wang, W., HU, Y. J., and Ling, L. 2013. Method and Implementation of Substructure FRF Synthesis Considering Connection Property. *China Mechanical Engineering*. 24: 1385-1389.
[22] Sheng, Z., Xie, S. Q., and Pan, C. Y. 2008. Probability Theory and Mathematical Statistics. Higher Education Press.